American Mineralogist, Volume 82, pages 697–707, 1997

The synthetic Cr^{2+} silicates $BaCrSi_4O_{10}$ and $SrCrSi_4O_{10}$: The missing links in the gillespite-type $ABSi_4O_{10}$ series

RONALD MILETICH, DAVID R. ALLAN,* AND ROSS J. ANGEL

Bayerisches Geoinstitut, Universität Bayreuth, D-95440 Bayreuth, Germany

ABSTRACT

The new Cr^{2+}–containing silicate compounds $BaCrSi_4O_{10}$ and $SrCrSi_4O_{10}$ were synthesized both from alkali-borate fluxes and by high-T subsolidus solid-state reactions. The gillespite-type crystal structures (space group $P4/ncc$, $Z = 4$) were determined from single-crystal X-ray diffraction data. The unit-cell parameters are $a = 7.4562(4)$, $c = 15.5414(4)$ Å for $SrCrSi_4O_{10}$, and $a = 7.5314(3)$, $c = 16.0518(4)$ Å for $BaCrSi_4O_{10}$. Comparison with previously published data shows that A (= Ba, Sr, Ca) cation substitution in $ABSi_4O_{10}$ gillespite-type compounds mainly affects the c lattice parameter whereas the substitution of the B (= Cu, Cr, Fe) site leads to only small changes, mainly in a. The Cr^{2+} cation occupies a square-planar coordinated site unique in oxide crystal chemistry, with a Cr–O bond length of 1.999 ± 0.002 Å in all three Cr compounds. The rigidity of these bonds leaves the $CrSi_4O_{10}$ layers within the structure with only one significant degree of freedom, that of rotation of the four-membered Si_4O_{10} rings in response to substitution on the A cation site. The magnitudes of these rotations are independent of the identity of the B cation. In addition the AO_8 polyhedron becomes more elongated // c with increasing radius of the A cation. The increasing aplanarity of the $O(3)X_3$ configuration is almost exclusively determined by occupational changes on A, whereas the aplanarity of the square-planar $BO(3)_4$ group can be related to the positional shifts induced by the individual substitutions on both A and B sites. Polarized optical absorption spectroscopy was conducted on ($hk0$) sections of $SrCrSi_4O_{10}$ and $BaCrSi_4O_{10}$. Absorption bands at ~19500, ~14900, and ~22070 cm^{-1} could be assigned to $^5B_{1g} \rightarrow {}^5B_{2g}$, $^5B_{1g} \rightarrow {}^5A_{1g}$ ($\mathbf{E} \perp c$), and $^5B_{1g} \rightarrow {}^5E_g$, ($\mathbf{E} // c$) spin-allowed d-d transitions for Cr^{2+} in a square-planar configuration. The crystal-field stabilization energies of 13110 ± 150 and 13220 ± 180 cm^{-1} are indistinguishable for both compounds reflecting the very similar CrO_4 geometries.

INTRODUCTION

Natural and synthetic gillespite undergo a pressure-induced, reversible first-order phase transition variously reported to occur between 1.2 and 1.8 GPa (Hazen and Burnham 1974; Huggins et al. 1975, 1976; Hazen 1977; Hazen and Finger 1983). The relative size of the A cation (that is Ba in gillespite), for which the number of coordinating O atoms increases from eight to ten, plays a key role in the phase transition (Hazen and Finger 1983). In addition, the phase transition is accompanied by, among other structural changes, a change from an unusual square-planar fourfold coordination to a more normal distorted (4 + 2) octahedral coordination. The color change at the phase transition was also the subject of speculation and was originally attributed by Strens (1966) to spin pairing accompanying a change in the crystal field from a high-to-low spin state. However, Abu-Eid et al. (1973) later showed that the changes of the Fe^{2+} coordination and polyhedral distortion explain the transition-induced change in optical absorption.

As the square-planar coordination geometry is an extreme version of a uniaxially elongated octahedron, which is expected to be favored by Jahn-Teller–active cations like Cu^{2+} and Cr^{2+}, the existence of an isostructural $ABSi_4O_{10}$ series (A = Ba, Sr, Ca; B = Cu^{2+}, Cr^{2+}) is to be expected. Although all three Cu compounds are known to exist, both as synthetic phases (Janzcak and Kubiak 1992; Lin et al. 1992; Chakoumakos et al. 1993) and as the natural minerals effenbergerite, wesselsite, and cuprorivaite (Giester and Rieck 1994, 1996; Pabst 1959), the existence of only one Cr^{2+} analog, $CaCrSi_4O_{10}$, was reported previously (Gasparik 1981; Belsky et al. 1984). To determine the influence of the type B cations on the gillespite-type crystal structure, we synthesized the two missing Cr^{2+} phases and determined their crystal structures from single-crystal X-ray diffraction data. The seven known compounds with the gillespite structure type were compared to identify the mechanisms of structural changes induced by the substitution on the two cation

* Present address: Department of Physics and Astronomy, The University of Edinburgh, Edinburgh EH9 3JZ, U.K.

0003–004X/97/0708–0697$05.00

TABLE 1. Crystal data and details of data reduction and least-squares refinements

	$BaCrSi_4O_{10}$	$SrCrSi_4O_{10}$	$CaCrSi_4O_{10}$
M_r (g)	461.67	411.95	364.41
a (Å)	7.5314(3)	7.4562(4)	7.3772(7)
c (Å)	16.0518(4)	15.5414(4)	15.1231(8)
V (Å^3)	910.49(6)	864.02(9)	823.05(13)
D_x (g/cm^3)	3.368	3.167	2.941
μ (Mo$K\alpha$) (cm^{-1})	60.23	78.04	25.82
Dimensions (μm)	70 × 70 × 35	84 × 85 × 25	64 × 68 × 14
Reflections measured	2309	2269	2082
Transmission factors	0.661–0.816	0.541–0.762	0.821–0.977
Unique reflections (4/*mmm*)	1007	953	906
Reflections with $F > 4\sigma_F$	585	526	324
$R_{int}(F > 0\sigma)$, $R_{int}(F > 4\sigma)$	0.053, 0.027	0.076, 0.036	0.086, 0.042
N_{obs}/N_{var}	13.5	15.0	8.3
R, $R_w(F > 4\sigma_F)$*	0.030, 0.035	0.035, 0.041	0.048, 0.055
Gof†	1.02	0.90	1.23

* $R = [\Sigma w(|F_o| - F_c|)/\Sigma wF_o]$; $R_w = [\Sigma w(|F_o| - |F_c|)^2/\Sigma wF_o^4]^{1/2}$; $w = [\sigma^2(F_o) + (pF_o)^2]^{-2}$ ($p = 0.01$).
† Gof = $[\Sigma w(|F_o| - |F_c|)^2/(N_{obs} - N_{var})]^{1/2}$.

sites. Information about the synthesis and preliminary X-ray powder data were given by Miletich and Allan (1996).

EXPERIMENTAL METHODS

Synthesis

Single crystals of $ACrSi_4O_{10}$ (A = Ba, Sr, Ca) were synthesized from ACO_3 (A = Ba, 99.999%, Alfa; A = Sr, 99.99%, Aldrich, A = Ca, 99.99%, Aldrich), Cr_2O_3 (99.0%, Alfa), Cr metal (99.5%, 2 μm, Johnson Matthey), and SiO_2 (99.9%, 325 mesh, Alfa). A homogeneous mixture of $1ACO_3 + 4SiO_2$ was first ignited at $T = 1100$ °C for 24 h and then $0.33Cr_2O_3$ and $0.5Cr^0$ were added to yield a $1.0AO{\cdot}1.0CrO{\cdot}4.0SiO_2{\cdot}0.16Cr^0$ bulk composition. Depending on the individual experiment, small amounts of additional SiO_2 (Belsky et al. 1984), a $BaO + B_2O_7$ mixture, $Li_2B_4O_7$ (99.9%, Aldrich), or $Na_2B_4O_7$ (98%, Merck) was added to act as flux (Pabst 1959). Homogeneous mixtures of these reactants were placed in Cr metal capsules, which were manufactured from Cr metal rod (99.7%, Metallwerk Plansee, Reutte, Austria). The sample capsules were sealed in evacuated quartz-glass tubes ($P < 10^{-4}$ bar) and heated to temperatures in the range 840–1020 °C (low-T experiments of samples containing borate flux) or to 1400° or 1450 °C (high-T experiments for the subsolidus solid-state reactions) for 1–120 h. The excess of Cr metal in all experiments ensured that the oxygen fugacities were held below the Cr^0–Cr_2O_3 buffer conditions (Gasparik 1981; de Villiers and Muan 1992; Nell and de Villiers 1993; Li et al. 1995). The f_{O_2} values in our synthesis experiments were estimated to be approximately 10^{-27}–10^{-19} bar, and 10^{-15}–10^{-14} bar for the 800–1020 °C and 1350–1450 °C T ranges, respectively (Holzheid and O'Neill 1995). High-T experiments were

TABLE 2. Fractional coordinates and anisotropic displacement parameters ($\beta_{ij} \times 10^3$) for $BaCrSi_4O_{10}$, $SrCrSi_4O_{10}$, and $CaCrSi_4O_{10}$

Atom	Site	Point symm.	x/a	y/b	z/c	β_{11}	β_{22}	β_{33}	β_{12}	β_{13}	β_{23}	β_{eq}
						$BaCrSi_4O_{10}$						
Ba	4*b*	$\bar{4}$ . .	¼	¾	0	6.51(6)	= β_{11}	1.17(2)	0	0	0	1.39
Cr	4*c*	4 . .	¼	¼	0.09181(10)	4.19(11)	= β_{11}	1.70(5)	0	0	0	1.23
Si	16*g*		0.51961(17)	0.93512(17)	0.15441(8)	4.91(19)	4.93(18)	1.12(4)	0.32(16)	0.07(8)	−0.08(8)	1.13
O1	8*f*	. . 2	= *y* − ½	0.97275(64)	¼	15.30(87)	= β_{11}	1.26(15)	−2.02(99)	1.40(31)	= $-\beta_{13}$	2.74
O2	16*g*		0.72301(48)	0.99639(50)	0.13722(22)	4.44(61)	9.51(70)	2.03(12)	−0.74(44)	−0.07(22)	0.67(24)	1.75
O3	16*g*		0.39096(54)	0.02503(51)	0.08973(23)	7.01(59)	5.44(58)	2.55(15)	1.22(43)	−1.51(24)	−0.66(25)	1.82
						$SrCrSi_4O_{10}$						
Sr	4*b*	$\bar{4}$ . .	¼	¾	0	5.18(8)	= β_{11}	1.28(3)	0	0	0	1.18
Cr	4*c*	4 . .	¼	¼	0.08564(9)	3.68(12)	= β_{11}	1.64(5)	0	0	0	1.07
Si	16*g*		0.50962(17)	0.92707(17)	0.15094(8)	3.60(17)	4.28(17)	1.24(4)	0.01(14)	0.10(7)	−0.02(8)	0.98
O1	8*f*	. . 2	= *y* − ½	0.96361(58)	¼	11.02(65)	= β_{11}	1.73(17)	−1.31(75)	1.17(28)	= $-\beta_{13}$	2.20
O2	16*g*		0.71284(44)	0.99735(55)	0.13192(21)	4.34(56)	8.42(65)	1.86(12)	−0.94(43)	−0.26(19)	0.62(24)	1.54
O3	16*g*		0.37015(44)	0.01058(46)	0.08572(23)	4.60(50)	3.85(50)	2.52(13)	1.30(42)	−1.14(22)	0.51(24)	1.44
						$CaCrSi_4O_{10}$						
Ca	4*b*	$\bar{4}$ . .	¼	¾	0	5.17(25)	= β_{11}	2.46(12)	0	0	0	1.50
Cr	4*c*	4 . .	¼	¼	0.07914(17)	3.92(20)	= β_{11}	2.76(11)	0	0	0	1.41
Si	16*g*		0.50303(28)	0.92233(27)	0.14768(14)	4.30(30)	4.23(29)	2.48(9)	−0.05(25)	−0.01(17)	−0.18(17)	1.37
O1	8*f*	. . 2	= *y* − ½	0.95734(85)	¼	11.47(1.12)	= β_{11}	2.48(32)	−0.89(1.24)	0.78(51)	= $-\beta_{13}$	2.42
O2	16*g*		0.70527(61)	0.99877(83)	0.12658(35)	3.87(94)	8.63(99)	3.64(27)	−0.95(68)	0.16(42)	−0.58(54)	2.02
O3	16*g*		0.35742(63)	0.00147(71)	0.08218(35)	4.94(81)	4.82(78)	3.36(25)	0.59(73)	−0.12(46)	0.50(51)	1.73

Note: Estimated standard deviations are given in parentheses, anisotropic displacement parameters are given in the form $\exp[-(h^2\beta_{11} + k^2\beta_{22} + l^2\beta_{33} + 2hk\beta_{12} + 2hl\beta_{13} + 2kl\beta_{23})]$ (space group *P*4/*ncc*, origin at $\bar{1}$; $Z = 4$).

TABLE 3. Selected interatomic distances (Å), bond angles (°), polyhedral volumes (Å^3), and polyhedral distortion parameters for $ACr^{2+}Si_4O_{10}$ (A = Ba, Sr, Ca)

	$BaCrSi_4O_{10}$	$SrCrSi_4O_{10}$	$CaCrSi_4O_{10}$
A-O2 × 4	2.737(4)	2.521(3)	2.369(5)
A-O3 × 4	2.923(4)	2.798(4)	2.685(4)
V_{poly}	36.18	30.14	25.96
$\Delta^{[8]}$*	0.0011	0.0027	0.0039
σ^2_{Cube}†	186.3	121.5	76.7
Cr-O3 × 4	2.000(4)	1.998(3)	1.998(5)
$\Delta z_{(Cr,O)}$‡	0.038(4)	0.002(4)	−0.046(6)
O3-Cr-O3^{cis} × 4	89.98(16)	90.00(14)	89.97(20)
O3-Cr-O3^{trans} × 2	177.80(18)	180.00(25)	177.36(26)
Si-O3	1.573(4)	1.578(4)	1.574(5)
Si-O1	1.599(3)	1.601(3)	1.605(4)
Si-O2	1.624(4)	1.626(4)	1.627(5)
Si-O2′	1.626(4)	1.630(4)	1.633(5)
V_{poly}	2.12	2.13	2.13
q.e.†	1.0024	1.0028	1.0033
σ^2_{Tet}	9.70	10.79	12.47
Σ X-O1-X§	176.29(36)	176.44(33)	176.02(46)
Σ X-O2-X§	359.83(35)	359.96(36)	360.00(39)
Σ X-O3-X§	354.17(35)	357.94(33)	359.30(49)

Note: Estimated standard deviations are given in parentheses.

* $\Delta^{[8]}$ = mean-square relative deviation from average bond length for eightfold coordination (Brown and Shannon 1973).

† q.e. = quadratic elongation, σ^2 = bond-angle variance (Robinson et al. 1971).

‡ $\Delta z_{(Cr,O)}$ = aplanarity of the CrO_4 group.

§ X = Si for O1$^{[2Si]}$; X = Si, A for O2$^{[2Si+1A]}$; X = Si, A, Cr, for O3$^{[1Si+1A+1Cr]}$.

cooled at 1 °C/min for 100 min and then quenched by withdrawing the sample assembly from the furnace; low-T experiments were slowly cooled to room temperature over a period of 36 h starting with a maximum cooling rate of about 12 °C/min.

To prepare the samples for characterization by X-ray diffraction the compact experiment products were treated with dilute 0.1 M HCl to remove the remnant borate flux as well as the excess of Cr metal. The experiment products mainly consisted of pink to salmon-red aggregates of platy, subhedral $ACrSi_4O_{10}$ crystals. Their morphology

TABLE 4. Calculated bond valences v (v.u.) for $ACr^{2+}Si_4O_{10}$ (A = Ba, Sr, Ca)

	$BaCrSi_4O_{10}$	$SrCrSi_4O_{10}$	$CaCrSi_4O_{10}$
v(A-O2) × 4	0.295(7)	0.336(8)	0.338(6)
v(A-O3) × 4	0.178(4)	0.159(4)	0.144(3)
Σv(A-O)	1.89(4)	1.98(5)	1.93(4)
v(Cr-O3) × 4	0.482(18)	0.485(17)	0.485(20)
Σv(Cr-O)	1.93(8)	1.94(7)	1.94(8)
v(Si-O3)	1.148(15)	1.132(15)	1.145(18)
v(Si-O1)	1.070(11)	1.064(12)	1.053(15)
v(Si-O2)	1.000(15)	0.995(15)	0.992(18)
v(Si-O2′)	0.995(15)	0.984(15)	0.976(18)
Σv(Si-O)	4.21(6)	4.18(6)	4.17(7)
Σv(O1-X*)	2.14(3)	2.13(3)	2.11(3)
Σv(O2-X*)	2.18(4)	2.14(4)	2.11(4)
Σv(O1-X*)	1.92(4)	1.95(4)	1.97(5)

Note: Estimated standard deviations are given in parentheses. Bond valences were calculated using the R_{ij} parameters of Brese and O'Keeffe (1991), errors were propagated from the $\sigma(R_{ij})$ given by Brown and Altermatt (1985) and the estimated standard deviations for the bond lengths. $\sigma(R)$ for Cr^{2+}-O was assumed to be 0.01.

* X = Si for O1$^{[2Si]}$; X = Si, A for O2$^{[2Si+1A]}$; X = Si, A, Cr for O3$^{[1Si+1A+1Cr]}$.

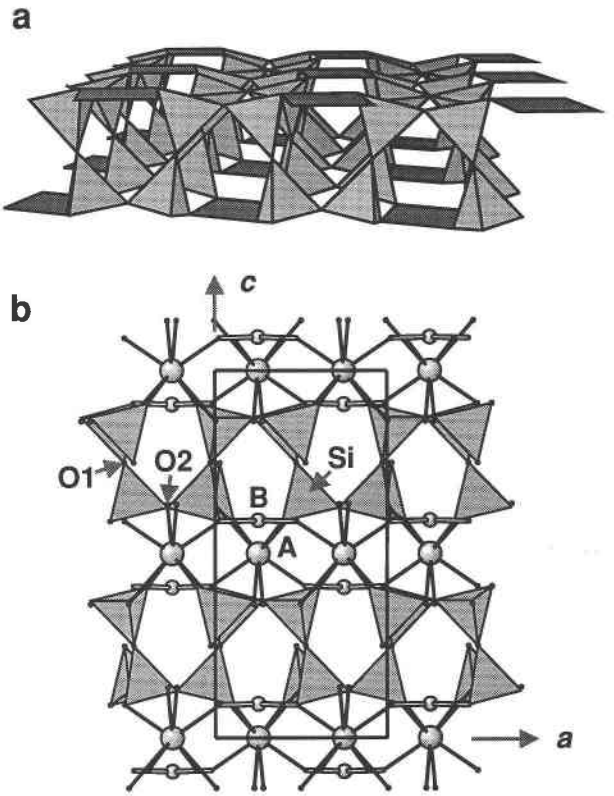

FIGURE 1. The $ABSi_4O_{10}$ structure type. (**a**) the $[BSi_4O_{10}]^{2-}$ sheet (**b**) structure projection down the a axis (graphical displays with ATOMS: Dowty 1995).

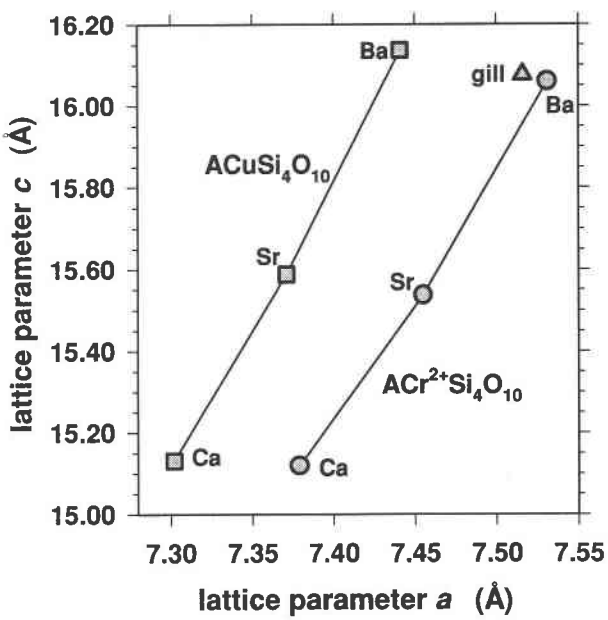

FIGURE 2. Lattice parameters a and c for the $ABSi_4O_{10}$ phases: B = Cr^{2+} (circles), = Cu^{2+} (squares), = Fe^{2+} (triangle). Phases with the same B cations are connected by tie lines; gill = gillespite, $BaFe^{2+}Si_4O_{10}$. Data for B = Cu^{2+} and Fe^{2+} from Chakoumakos et al. (1993) and Hazen and Finger (1983), respectively.

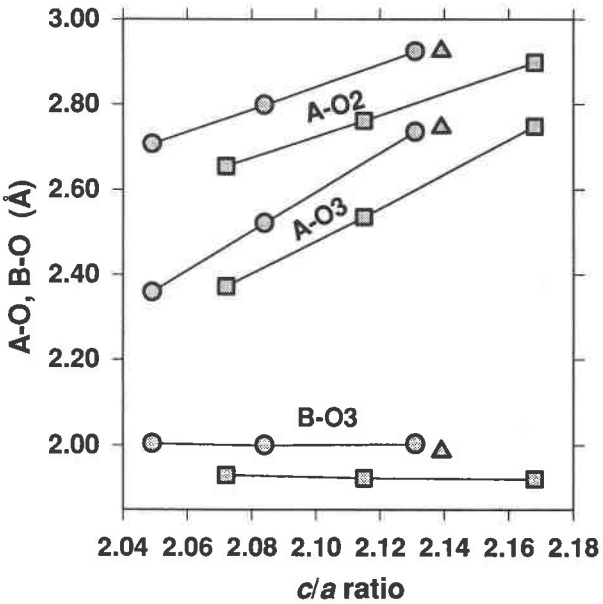

FIGURE 3. Variation of A–O and B–O bond distances in gillespite structures. (Symbol notation: see Fig. 2).

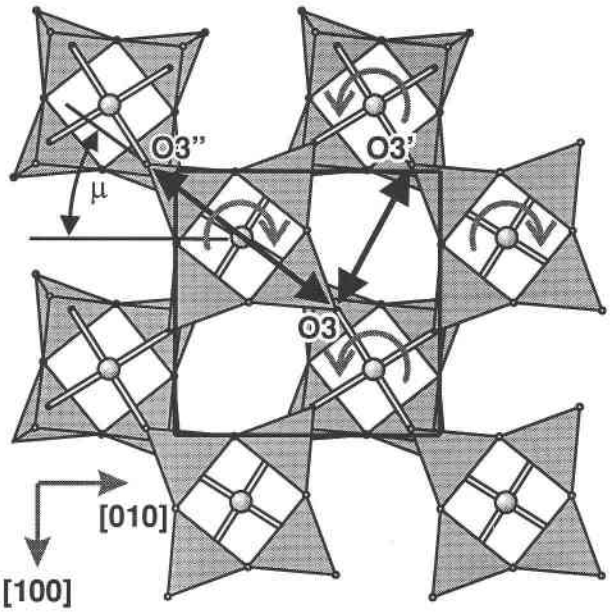

FIGURE 4. Rotation mechanism within the BSi_4O_{10} sheet induced by the substitution of Ba for Ca on the A cation site. As the A cation size is increased, the O3···O3′ intrapolyhedral distance (arrowed line) of the AO_8 square anti-prism increases resulting in rotation of the four-membered Si_4O_{10} rings and the BO_4 groups. The degree of rotation is measured by the angle μ as defined between the intra-ring O3···O3″ and the crystallographic [100] directions. Edges of the square box correspond to the tetragonal unit cell (projection down the *c* axis).

was dominated by {001}, {110}, and {102} faces. The single crystals used for the data collection and structure refinements reported here were all obtained from the high-*T* solid-state experiments at 1400–1450 °C. Experimental products were identified by X-ray powder diffraction with a STOE STADI-P diffractometer equipped with a linear position-sensitive detector and operated in transmission-mode geometry using Co$K\alpha_1$ (λ = 1.78897 Å) radiation obtained with a curved Ge(111) monochromator. All XRD patterns were recorded with 0.5° increments of the PSD and counting times of 50–120 s per step in the range 5–100° 2θ. In addition to the gillespite phases, experimental products included metallic Cr, quartz, tridymite, or cristobalite, Cr_2O_3, $Ca_3Si_3O_9$ (wollastonite), $\alpha-Sr_3Si_3O_9$, and $\beta-BaSi_2O_5$. Precise lattice parameters of the gillespite phases were obtained by least-squares refinements of 18–29 accurate 2θ values in the 12–70° 2θ range using NBS 640 Si added as an internal standard.

Single-crystal X-ray diffraction

Specific data for the crystals used for the single-crystal data collections are given in Table 1. X-ray diffraction intensities were collected (at room temperature, 21 °C) on an Enraf Nonius CAD4 four-circle diffractometer with graphite-monochromatized Mo$K\alpha$ radiation (λ = 0.7107 Å) with a tube power of 50 kV and 50 mA. X-ray intensities were collected to $(\sin\theta)/\lambda \leq 0.807$ Å^{-1} within one octant of reciprocal space (with $0 \leq h \leq 12$, $0 \leq k \leq 12$, $0 \leq l \leq 25$) by ω scans (scan width: 0.66° + 0.35° tan θ). Three standard reflections serving as intensity and orientation controls were monitored every 2 h.

Integrated X-ray intensities were obtained from the scan data using a modified Lehmann-Larsen algorithm (Grant and Gabe 1978). Intensities of all measured reflections were then corrected for Lorentz and polarization effects and crystal absorption (according to the optically determined crystal shape) using a modified version of ABSORB (Burnham 1966). Data reduction confirmed the systematic absence conditions for the space-group *P*4/*ncc*. All symmetry-allowed reflections were averaged using the criteria of Blessing (1987) for averaging and re-

TABLE 5. Selected interatomic distances and rotation angle μ of the Si_4O_{10} rings in $ABSi_4O_{10}$ compounds

	Ba-Cr	Sr-Cr	Ca-Cr	Ba-Cu	Sr-Cu	Ca-Cu	Ba-Fe
O3···O3′ (Å)	4.655(5)	4.279(5)	4.035(7)	4.662(2)	4.294(2)	4.042(2)	4.662(3)
O3···O3″ (Å)	6.810(5)	6.869(5)	6.879(7)	6.835(2)	6.885(2)	6.901(2)	6.818(3)
μ (°)	37.45(9)	34.45(9)	32.62(12)	37.82(6)	34.85(6)	32.92(6)	37.56(7)

Notes: O3···O3′ = inter-ring distance underneath the A site; O3···O3″ = intra-ring distance equivalent to the Si_4O_{10} ring diameter; μ = angle between the O3···O3″ direction and the crystallographic *a* axis.

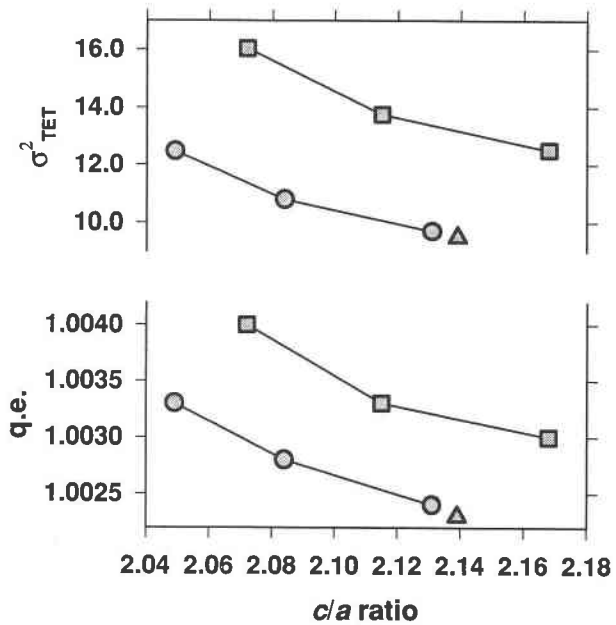

FIGURE 5. Variation of the SiO_4 quadratic elongation q.e. = $\frac{1}{4}\Sigma\ (l_i/l_0)^2$ and the bond-angle variance σ^2 (see Robinson et al. 1971). Symbols notation: see Figure 2.

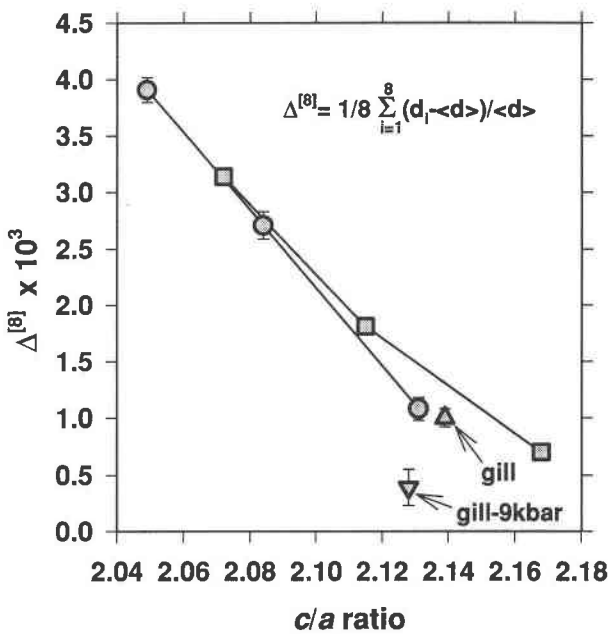

FIGURE 7. Variation of the AO_8 bond-length distortion parameter $\Delta^{[8]}$ (Brown and Shannon 1973). <d> = mean A-O bond distance; symbol notation: see Figure 2.

jection of outliers. Structure refinements were conducted with RFINE90, a development version of RFINE4 (Finger and Prince 1975). A weight of $w = [\sigma^2(F_o) + (pF_o)^2]^{-2}$ ($p = 0.01$) was assigned to each observed reflection, where $\sigma(F_o)$ was derived from counting and averaging statistics. The positional parameters for effenbergerite (Giester and Rieck 1994) and $CaCrSi_4O_{10}$ (Belsky et al. 1984) were used as starting models. Complex scattering factors for neutral atoms, as well as the linear mass-absorption coefficients, were taken from the *International Tables of Crystallography* (Maslen et al. 1992; Creagh and McAuley 1992). A correction for secondary isotropic extinction (Lorentzian type-I distribution; Becker and Coppens 1974) resulted in insignificantly small values of the extinction parameter and this was therefore omitted from the final refinements. The results of the least-squares refinements (38 variable parameters) are given in Table 1, and the refined structural parameters are summarized in Table 2. Our data for the Ca-Cr compound do not differ significantly from those reported by Belsky et al. (1984).

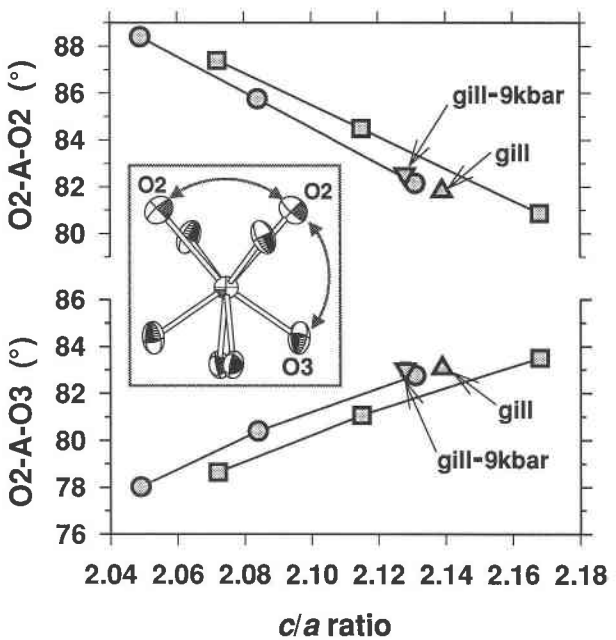

FIGURE 6. Variation of selected O–A–O bond angles within the $^{[8]}AO_8$ polyhedron (Symbol notation: see Fig. 2; gill = gillespite, gill-9kbar = gillespite at 9 kbar; the inset shows the AO_8 coordination in a projection down the *a* axis).

The single-crystal unit-cell parameters were determined from the setting angles of 32 reflections between 17.0 and 28.8° 2θ determined on a customized Huber four-circle diffractometer operated with non-monochromatized Mo X-ray radiation (Angel et al. 1997). To prevent crystal-offset errors and diffractometer aberrations affecting the results, the technique of diffracted-beam centering (King and Finger 1979) was used to obtain corrected setting angles. Unconstrained unit-cell parameters corresponded to tetragonal symmetry, within 1.5 estimated standard deviations (esds), and the unit-cell parameters, constrained to tetragonal symmetry and obtained by vector-least-squares fit to the reflection positions (Ralph and Finger 1982), are reported in Table 1.

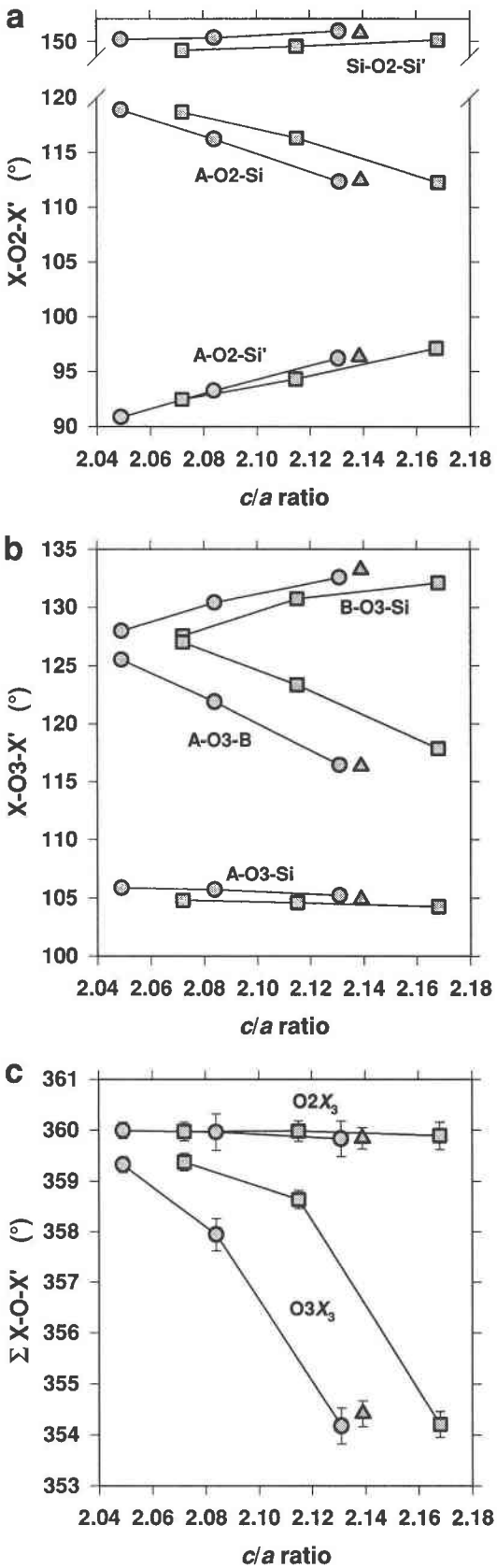

FIGURE 8. Variation of the (a) X–O2–X′, (b) X–O3–X′ bond angles, and (c) their sums Σ (X–O2–X′) and Σ (X–O3–X′). X, X′ = Si, A, B; symbol notation: see Figure 2.
←

Optical absorption spectroscopy

To record electronic absorption spectra from 10 000 to 27 500 cm^{-1}, doubly-polished (*hk*0) platelets with a thickness of 26 and 28 μm, respectively, were prepared from platy crystals (approximately 100 × 100 × 30 μm) of the Sr and Ba compounds oriented by the X-ray oscillation film method to better than 0.3°. The optical absorption measurements were made using a Bruker A590 microscope attached to a Bruker IFS 120 HR infrared spectrometer. Due to the small sample size the spot size of the beam was only 20 and 25 μm in diameter, which explains the poor signal-to-noise ratio, particularly for $SrCrSi_4O_{10}$. From every sample two spectra in different wavelength ranges (10 000 to 15 000 and 12 500 to 27 500 cm^{-1}) were accumulated and merged into the final spectrum. Each spectrum was averaged from 600 scans, and the spectral resolution was 4 cm^{-1}. Depending on the spectral range, different light sources (tungsten lamp, xenon arc lamp), beamsplitters (Si-coated CaF_2 or quartz), and detectors (narrow-band MCT or Si diode) were used.

Results and Discussion

$ABSi_4O_{10}$ structure type

The main feature of the topology of the gillespite structure type is the presence of two-dimensional infinite $[BSi_4O_{10}]_n$ layers parallel to (001) (Fig. 1). These composite layers are then connected in the [001] direction by interlayer A cations that occupy an eightfold-coordinated, distorted square-antiprismatic site with point symmetry 4. The response of the gillespite structure type to pressure (Hazen and Finger 1983) and cation substitution on the A (A = Ba, Sr, Ca) and B (B = Cr, Fe, Cu) sites is therefore a reflection of the strong bonding and steric hindrance within the $[BSi_4O_{10}]_n$ layer and the relatively weaker and less-constrained linkages (by means of the A cations) between the layers.

The detailed structure of these two-dimensional infinite $[BSi_4O_{10}]_n$ layers consists of silicate tetrahedra arranged in four-membered Si_4O_{10} rings. The bridging O atom within this ring is designated O2, and the connection of the Si_4O_{10} rings to an unbranched single-layer silicate $[Si_4O_{10}]_n$ sheet is achieved by means of the O1 atoms (Fig. 1). The structural topology of the silicate sheet can be described as two-dimensionally corrugated along [100] and [010]. The B cation occupies a square-planar site coordinated by four O3 atoms that are nonbridging corners of the SiO_4 tetrahedra, with all four B-O3 bonds lying in the (001) plane. These $BO(3)_4$ groups fit into the silicate sheet above the topological troughs of the silicate sheet.

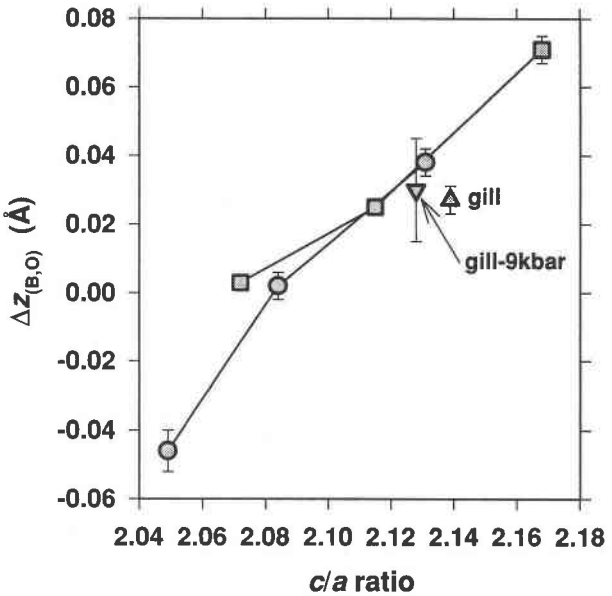

FIGURE 9. Variation of the BO_4 aplanarity: $\Delta z_{(B,O)} = c \cdot [z/c(B) - z/c(O3)]$. Symbol notation: see Figure 2.

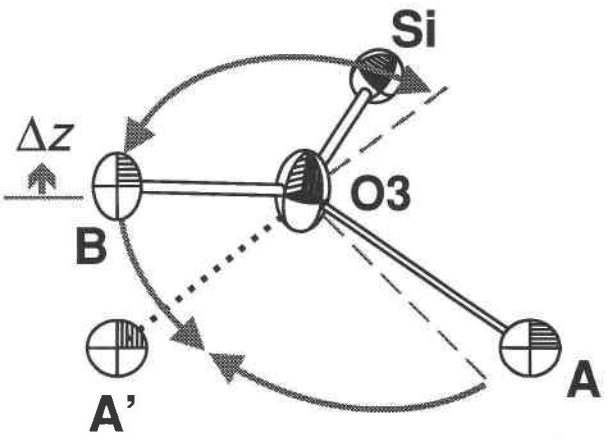

FIGURE 10. Changes on the $O(3)X_3$ geometry induced by the substitution of Ba for Ca. The dotted line represents the weak A′–O3 bond, which leads to the (3+1) configuration in orthorhombic gillespite. The dashed lines represent the positions of the A–O3 and Si–O3 bonds for A = Ba. Δz is the vector that decribes the aplanarity of the BO_4 group, which results from the positional shifts of O3 relative to B induced by the changes of the A–O3–B and Si–O3–B angles. Projection down the *a* axis.

Unit-cell parameters of $ABSi_4O_{10}$ compounds

Figure 2 shows a plot of *a* vs. *c* lattice parameters for all known gillespite-type $ABSi_4O_{10}$ compounds including the data for synthetic $ACuSi_4O_{10}$ of Chakoumakos et al. (1993) and those of the low-pressure polymorph of gillespite itself (Hazen and Finger 1983). Comparison of the structures that we have determined for the Cr compounds with those of the Cu and Fe compounds shows that when the larger Cr and Fe cations are substituted for Cu the length of the *a* unit-cell parameter increases as a direct result of the changes in the B–O bond length. Because the $BO(3)_4$ groups lie parallel to (001) the *c* unit-cell parameter is not affected significantly by the B site substitution. In contrast, the substitution of type A cations affects both the *a* and *c* lattice parameters with the changes in *c* dominating over those in *a* (Fig. 2). This effect can be explained by the fact that perpendicular to the plane of the $[BSi_4O_{10}]_n$ layer there are no external constraints on the AO_8 polyhedra, and therefore the interlayer spacing is more flexible in comparison with the changes induced within the (more or less) rigid BSi_4O_{10} sheets. Consequently, the *c*/*a* ratio can be used as a sensitive indicator of structural changes induced by independent A and B cation substitutions in the gillespite-type structure.

Structural changes induced by cation substitution

Comparison of the bond lengths, bond angles, and bond valences of the three Cr compounds (Tables 3 and 4) and the Cu and Fe compounds (Chakoumakos et al. 1993; Hazen and Finger 1983) shows that substitution at the A site, even with an increase of ~27% in the cation radius from Ca to Ba (Shannon 1976), has no significant effect on the B–O bond distance within the BSi_4O_{10} layer (Fig. 3). The rigidity of the BO_4 group, together with fourfold symmetry of the structure, leaves the layer with only one significant degree of freedom, that of rotation of the four-membered tetrahedral rings and the counter-rotation of the BO_4 groups themselves. Thus, as the radius of the A cation is increased, the O3···O3′ distance underneath the A site also increases as a result of the rotation of the tetrahedral rings (Fig. 4). This rotation, amounting to approximately 5° in both the Cu and the Cr compounds for the substitution of Ba for Ca (Table 5) is responsible for the increase in the *a* unit-cell parameter related with the A site substitution. Accompanying this rotation is a small decrease of the diagonal of the SiO_4 ring (as measured by the O3···O3″ distance across the ring) and a marginal decrease in the distortion of the SiO_4 tetrahedra with increasing A cation size (Fig. 5). Both the Si–O1–Si and Si–O2–Si bond angles remain invariant (within ± 1°) within all of the known gillespite-type structures, indicating the rigidity of the tetrahedral rings toward distortion and the rigidity of the corrugations of the silicate components of the BSi_4O_{10} layer.

Perpendicular to the the plane of the composite layers there are no external constraints on the AO_8 polyhedra, which therefore exhibit distortional changes predominantly along [001] with varying cation size. The variation of the individual O2–A–O2 and O2–A–O3 angles (Fig. 6) and the deviations from the ideal values within an undistorted cube (109.47 and 70.53°) clearly show that the AO_8 polyhedron elongates // *c* as the A cation size increases, also leading to an increase in the bond-angle variance of the site (see σ^2: Table 3), and a large increase in the *c* unit-cell parameter. Simultaneously, the AO_8 polyhedral bond-length distortion decreases (Fig. 7),

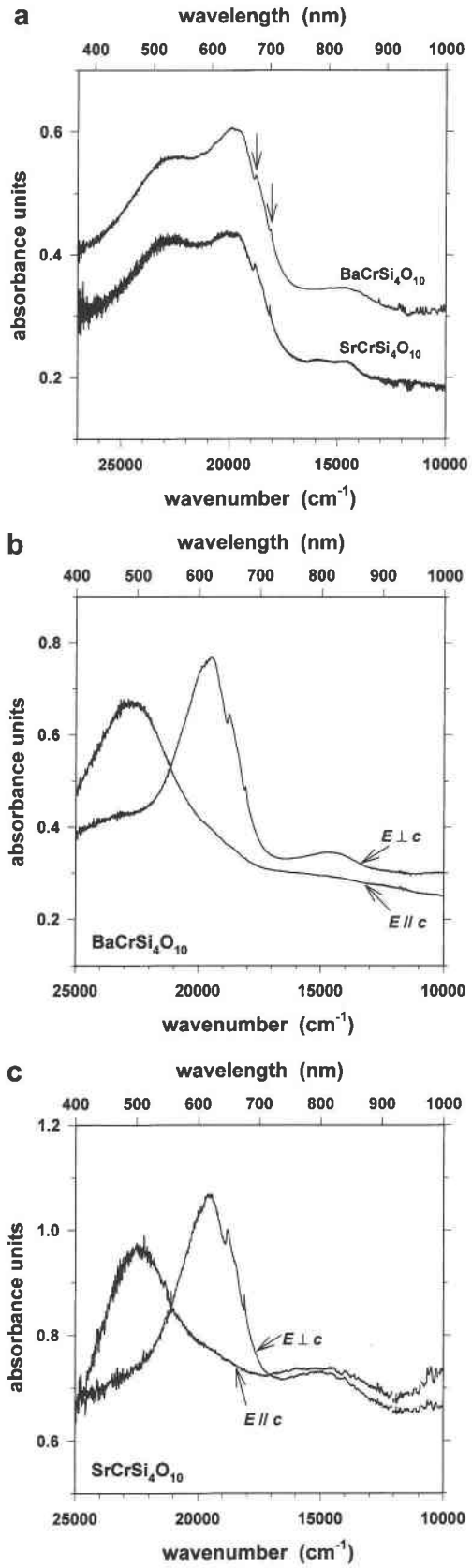

FIGURE 11. Electronic absorption spectra of $ACrSi_4O_{10}$ (A = Ba, Sr): unpolarized spectra (**a**), and polarized spectra (**b**, **c**). Arrows indicate bands assigned to d-d transitions arising through vibronic coupling.

←

which is the same behavior observed with increasing pressure in gillespite itself (Hazen and Finger 1983).

Significant changes are induced in the O atom configurations, in particular for O3, by cation substitution (Fig. 8a–c). The increase in the aplanarity of the $O(3)X_3$ configuration (see Fig. 8c) also follows the substitution at the A site. This increase might indicate that there is a tendency toward a (3 + 1) coordination, which exists for the high-pressure polymorph of gillespite, in which additional Ba–O3 bonds lead to a BaO_{10} coordination (Hazen and Finger 1983). The individual A–O3 and B–O3 bond lengths are responsible for changes in B–O3–X (X = A, Si) bond angles, which can be related both to the magnitude and to the direction of the BO_4 aplanarity (Fig. 9). The latter can be quantified by the separation along the c axis of the central B cation from the coordinating O3 atoms, given by $\Delta z_{(B,O)} = c\cdot[z/c(B) - z/c(O3)]$. Figure 10 displays the changes in the $O(3)X_3$ geometry from the O3 positional shifts induced by A + B cation substitution. For both the Cu and Cr compounds the aplanarity increases significantly with increasing cation radius of A, although this increase is approximately twice as large in the Ba–Cu compound as in the Ba–Cr compound and the BO_4 groups are (within the uncertainties) planar in the Ca–Cu and Sr–Cr structures. Thus the CrO_4 group in the Ca–Cr compound has the opposite distortion from planarity as that of all the other compounds.

Cr^{2+} coordination

Cr^{2+} normally occurs in oxides in distorted octahedral coordination by O as a result of Jahn-Teller distortion of the high-spin d^4 configuration in an octahedral crystal field. This uniaxial distortion occurs in almost all Cr^{2+}–containing sulfate and phosphate compounds

TABLE 6. The d-d band position after deconvolution of the $ACrSi_4O_{10}$ spectra

Band assignment	E // c	E ⊥ c	A^{2+}	Position (cm^{-1})	FWHM (cm^{-1})	ε (L mol/ cm^{-1})
$^5B_{1g} \rightarrow {}^5E_g$ (ν_1)	s	fb	Ba	22690 ± 80	2580	17.8
			Sr	22850 ± 100	3020	10.3
$^5B_{1g} \rightarrow {}^5B_{2g}$ (ν_2)	fb	s	Ba	19510 ± 70	2450	19.3
			Sr	19520 ± 80	2640	18.3
$^5B_{1g} \rightarrow {}^5A_{1g}$ (ν_3)	fb	w	Ba	14860 ± 150	2680	2.2
			Sr	15090 ± 180	2820	3.6

Note: Term symbols used for uniaxially distorted octahedral crystal field (D_{4h} symmetry). **E** = electric field vector; band occurrences: fb = forbidden, s = strong, w = weak; FWHM = full width at half maximum, ε = linear molar extinction coefficient of Cr^{2+} as measured at the respective wavenumber; errors for the band positions are estimated standard deviations.

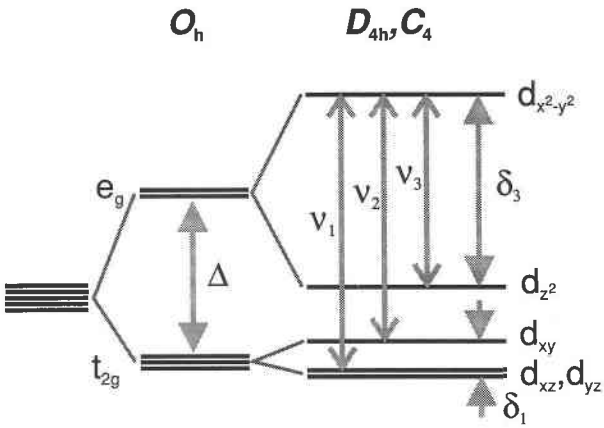

FIGURE 12. Energy-level diagram for Cr^{2+} in the square-planar site (C_4 symmetry) in gillespite-type $ACrSi_4O_{10}$. Energies for the electronic transitions ν_1 ($^5B_{1g} \rightarrow {}^5E_g$), ν_2 ($^5B_{1g} \rightarrow {}^5B_{2g}$), and ν_1 ($^5B_{1g} \rightarrow {}^5A_{1g}$), the crystal field splitting Δ, and the splittings of the e_g and t_{2g} orbitals (δ_3, δ_1) are given in Tables 6 and 7.

(Earnshaw et al. 1969; Ito et al. 1987; Vaalstra and Maslen 1987; Brynda et al. 1987; Dahmen et al. 1990; Figgis et al. 1990, 1991; Glaum 1992, 1993) with the mean $Cr^{2+}-O$ distance within the equatorial square ranging from 2.036 to 2.067 Å, whereas the average of the two axial distances ranges from 2.389 to 2.626 Å. In silicates, partial site occupation by Cr^{2+} was reported for the distorted octahedral sites in $(Mg,Cr)_2SiO_4$ olivine solid solutions with $X_{Cr^{2+}} < 0.25$ (Li et al. 1995) and $(Mg,Cr)SiO_3$ pyroxene solid-solutions with $X_{Cr^{2+}} < 0.75$ (Angel et al. 1989; Li et al. 1995).

More unusual Cr^{2+} coordinations include that of a square pyramid with four basal O atoms and one X atom at the apex of the CrO_4X polyhedra in the structures of $M(Cr_2Si_2O_7)_4X$ (M = Na, K; X = Cl, Br) (Schmidt and Glaum unpublished manuscript). The mean $Cr^{2+}-O$ distances in these compounds range from 2.006 to 2.020 Å and therefore fall between the values for the distorted octahedral configurations and the purely square-planar configuration found in the gillespite-structure type. Another fourfold planar O configuration was reported for Cr^{2+} in Cr_2SiO_4 (Dollase et al. 1994) in which the mean $Cr^{2+}-O$ distance was found to be 2.055 Å, but with two additional longer bonds ($Cr^{2+}-O$ = 2.72 Å) on one side of the equatorial plane completing the coordination.

The purely square-planar coordination in the gillespite-type structure ($Cr^{2+}-O$: 1.998–2.000 Å) is therefore unique among inorganic compounds, but can be considered to be equivalent to the geometry that would result from an extreme version of the Jahn-Teller distortion found in $Cr^{2+}O_6$ octahedra.

Electronic absorption spectroscopy

The electronic absorption spectra of $BaCrSi_4O_{10}$ and $SrCrSi_4O_{10}$ shown in Figure 11 are very similar to that given for $CaCrSi_4O_{10}$ (Belsky et al. 1984) and confirm the pleochroism that has been reported for isostructural compounds with Fe^{2+} and Cu^{2+} (Burns et al. 1966; Clark and Burns 1967; Ford and Hitchman 1979). Absorption bands of different intensities occur at ~14 900 and ~19 500 cm^{-1} for $\mathbf{E} \perp c$ polarization ($\mathbf{E}$ = electronic field vector), whereas the spectra with $\mathbf{E} \parallel c$ show only one main band centered at ~22 750 cm^{-1}. The exact positions of the different absorbance maxima, determined by deconvolution of Gaussian components, are summarized in Table 6.

TABLE 7. Crystal-field parameters of square-planar coordinated Cr^{2+} in $ACrSi_4O_{10}$

A^{2+}	Δ (cm^{-1})	δ_1 (cm^{-1})	δ_3 (cm^{-1})	CFSE (cm^{-1})
Ba	14200 ± 150	3180 ± 110	14860 ± 150	13110 ± 150
Sr	14195 ± 180	3330 ± 130	15090 ± 180	13223 ± 180
Ca	13780	2505	14925	12975

Notes: Δ = crystal-field splitting, δ_1 and δ_3 = energy separation within the t_{2g} and e_g levels, respectively. CFSE = crystal field stabilization energy. Values were calculated from the ν_1, ν_2, and ν_3 band positions given in Table 6 (and for $CaCrSi_4O_{10}$ from the data by Belsky et al. (1984) according to the following equations: $\Delta = \nu_1 - \frac{1}{2}\nu_3 - \frac{1}{3}\delta_1$; $\delta_1 = \nu_1 - \nu_2$; $\delta_3 = \nu_3$; CFSE = $\frac{2}{5}\Delta + \frac{1}{2}\delta_3$; errors were propagated from the estimated standard deviations of the band positions in Table 6.

Band assignment follows straightforward theoretical considerations based on the d-orbital geometries. The splitting of the ^5D ground term in an octahedral field results in an upper $^5T_{2g}$ level and a lower ^5E_g level, with one spin-allowed transition, corresponding to $^5E_g \rightarrow {}^5T_{2g}$. As the E_g ground term is orbitally degenerate for high-spin d^4, it is subject to Jahn-Teller distortion, giving a total of three spin-allowed transitions ($^5B_{1g} \rightarrow {}^5A_{1g}$, $^5B_{1g} \rightarrow {}^5B_{2g}$, $^5B_{1g} \rightarrow {}^5E_g$) for a uniaxial $O_h \rightarrow D_{4h}(C_4)$ distortion (see Fig. 12). The orientation and local symmetry of the $Cr^{2+}O_4$ group further simplifies prediction of the presence or absence of bands for the respective polarization directions by only allowing strong $^5B_{1g} \rightarrow {}^5E_g \parallel c$, strong $^5B_{1g} \rightarrow {}^5B_{2g} \perp c$, and weak $^5B_{1g} \rightarrow {}^5A_{1g} \perp c$ d-d absorptions. The actual acentric C_4 symmetry allows d-d transitions by the Laporte selection rule. Belsky et al. (1984) claimed that such absorptions can only occur through vibronic coupling as the $Cr^{2+}O_4$ group approaches centrosymmetric D_{4h} pseudosymmetry (see also Burns et al. 1966; Clark and Burns 1967; Ford and Hitchman 1979; Hitchman 1985). On the other hand, vibronic coupling is likely to be responsible for the weak bands that occur as at least two shoulders on the main $^5B_{1g} \rightarrow {}^5B_{2g}$ band at ~18 050 and ~18 800 cm^{-1} in our spectra (Fig. 11).

The crystallographic orientation and symmetry of the Cr^{2+} site allow the simple determination of the crystal-field splitting parameter Δ, of the $d_{xy} \leftrightarrow (d_{xz},d_{yz})$ (= δ_1) and $d_{z^2} \leftrightarrow d_{x^2-y^2}$ (= δ_3) energy separation, and thus the calculation of the crystal-field stabilization energies (CFSE) from Δ and δ_3. The values so calculated from the three absorption bands ν_1, ν_2, and ν_3 are given in Table 7.

CONCLUSIONS

The synthesis and determination of the structures of $BaCrSi_4O_{10}$ and $SrCrSi_4O_{10}$ have allowed, for the first

time, a complete systematic analysis of the response of the gillespite structure-type to cation substitution. In particular, the provision of data for the complete series of both $Cu^{2+}-$ (Chakoumakos et al. 1993) and $Cr^{2+}-$containing compounds has allowed us to identify clearly the separate responses of the structure type to substitutions on the A and B cation sites, and to show that it is unusual in that these responses are essentially independent of each other. That is, the structural response to cation substitution on the A site is essentially identical in both the Cu^{2+} and Cr^{2+} series of compounds. The study has also revealed the central role of O3 as the vital linch-pin of the entire structure, around which the BO_4 groups and the four-membered rings of silicate tetrahedra rotate to accommodate the A cation, and the detailed bonding requirements of which control the aplanarity of the BO_4 group.

All previous studies of the $ABSi_4O_{10}$ gillespite structure-type have reported *P4/ncc* symmetry (Pabst 1959; Hazen and Burnham 1974; Hazen 1977; Hazen and Finger 1983; Janczak and Kubiak 1992; Lin et al. 1992; Chakoumakos et al. 1993; Giester and Rieck 1994, 1996). Because careful examination of the X-ray diffraction peaks from our samples did not indicate any splitting of reflections, optical investigations of the (001) plates under crossed polarizers revealed no indication of any deviation from uniaxial optical character, and cell parameters and intensity data were consistent with Laue class *4/mmm* and space group *P4/ncc*, we also refined our structures in this space group. However, the significant deviations from the ideal bond-valence sums (Table 5), which are also present for the Cu^{2+} compounds (Chakoumakos et al. 1993), and the large anisotropic displacement parameters of the O atoms, in particular for O1, (Hazen and Finger 1983; Belsky et al. 1984; Giester and Rieck 1994, 1996; this work: Table 3) might indicate that the *P4/ncc* space-group symmetry is not the true symmetry for the low-pressure form of the $ABSi_4O_{10}$ structure, but represents an average structure from which small deviations of either a static or dynamic nature may occur.

Acknowledgments

We would like to thank Hubert Schulze for preparation of the samples for the optical measurements, and Hans Keppler and Marcus Nowak for obtaining and discussing the absorption spectra. Furthermore we would like to thank Robert Glaum (Giessen) for giving us access to structure data before publication.

References cited

Abu-Eid, R., Mao, H.K., and Burns, R.G. (1973) Polarized absorption spectra of gillespite at high pressure. Carnegie Institute Year Book, 72, 564–567.

Angel, R.J., Gasparik, T., and Finger, L.W. (1989) Crystal structure of a Cr^{2+} -bearing pyroxene. American Mineralogist, 74, 599–603.

Angel, R.J., Allan, D.R., Miletich, R., and Finger, L.W. (1997) The use of quartz as an internal pressure standard in high-pressure crystallography. Journal of Applied Crystallography, in press.

Becker, P.J. and Coppens, P. (1974) Extinction within the limit of validity of the Darwin transfer equations. I. General formalisms for primary and secondary extinction and their application to spherical crystals. Acta Crystallographica, A30, 129–147.

Belsky, H.L., Rossman, G.R., Prewitt, C.T., and Gasparik, T. (1984) Crystal structure and optical spectroscopy (300 to 2200 nm) of $CaCrSi_4O_{10}$. American Mineralogist, 69, 771–776.

Blessing, R.H. (1987) Data reduction and error analysis for accurate single crystal diffraction intensities. Crystallography Reviews,1, 3–58.

Brese, N.E. and O'Keeffe, M. (1991) Bond-valence parameters for solids. Acta Crystallographica, B47, 192–197.

Brown, I.D. and Altermatt, D. (1985) Bond-valence parameters obtained from a systematic analysis of the Inorganic Crystal Structure Database. Acta Crystallographica, B41, 244–257.

Brown, I.D. and Shannon, R.D. (1973) Empirical bond-strength-bond-length curves for oxides. Acta Crystallographica, A29, 266–282.

Brynda, J., Kratochvil, B., and Cisarova, I. (1987) The determination of crystal structure of chromium(II) phosphite dihydrate, $CrHPO_3{\cdot}2H_2O$. Collection of Czechoslovakian Chemical Communications, 52, 1742–1747.

Burnham, C.W. (1966) Computation of absorption corrections and the significance of end effects. American Mineralogist, 51, 159–167.

Burns, R.G., Clark, M.G., and Stone, A.J. (1966) Vibronic polarization in the electronic spectra of gillespite, a mineral containing iron(II) in square-planar coordination. Inorganic Chemistry, 5, 1268–1272.

Chakoumakos, B.C., Fernandez-Baca, J.A., and Boatner, L.A. (1993) Refinement of the structures of the layer silicates $MCuSi_4O_{10}$ (M=Ca,Sr,Ba) by Rietveld Analysis of Neutron Powder Diffraction Data. Journal of Solid State Chemistry, 103, 105–113.

Clark, M.G. and Burns, R.G. (1967) Electronic spectra of Cu^{2+} and Fe^{2+} square planar coordinated by oxygen in $BaXSi_4O_{10}$. Journal Chemical Society (A), 1967, 1034–1038.

Creagh, D.C. and McAuley, W.J. (1992) X-ray dispersion correction. In A.J.C. Wilson, Ed., International Tables for Crystallography—Volume C, p. 206–219. Kluwer Academic Publishers, Dordrecht.

Dahmen, T., Glaum, R., Schmidt, G., and Gruehn, R. (1990) Zur Darstellung und Kristallstruktur von $CrSO_4{\cdot}3H_2O$. Zeitschrift für Anorganische und Allgemeine Chemie, 586, 141–148.

Dollase, W.A., Seifert, F., and O'Neill, H.St.C. (1994) Structure of Cr_2SiO_4 and possible metal-metal interactions in crystals and melt. Physics and Chemistry of Minerals, 21, 104–109.

Dowty, E. (1995) Atoms for Windows, Version 3.1. Shape Software, Hidden Valley Road, Kingsport, U.S.A.

Earnshaw, A., Larkworthy, L.F., and Patel, K.C. (1969) Chromium(II) Chemistry. Part IV. Double sulphates. Journal of the Chemical Society, A 1969, 1334–1339.

Figgis, B.N., Kucharski, E.S., and Reynolds, P.A. (1990) Charge density in $(NH_4)_2Cr(SO_4)_2{\cdot}6H_2O$ at 84K: a Jahn-Teller distorted complex. Acta Crystallographica; B46, 577–586.

Figgis, B.N., Kucharski, E.S., and Forsyth, B. (1991) The structure of $(ND_4)_2Cr(SO_4)_2{\cdot}6D_2O$ at 4.3K by neutron diffraction. Acta Crystallographica, C47, 419–421.

Finger, L.W. and Prince, E. (1975) A system of Fortran IV computer programs for crystal structure computations. U.S. National Bureau of Standards Technical Note, 854, 128p.

Ford, R.J. and Hitchman, M.A. (1979) Single crystal electronic and EPR spectra of $CaCuSi_4O_{10}$, a synthetic silicate containing copper(II) in a four-coordinate, planar ligand environment. Inorganic Chimica Acta, 33, L167–L170.

Gasparik, T. (1981) Some phase relations involving chromous pyroxenes and other Cr^{2+} bearing phases at pressures less then 1 atmosphere. Proceedings of the 12th Lunar Science Conference, (abstract) Supplementum to Geochimica Cosmochimica Acta, Part 1, 333–335.

Glaum, R. (1992) Beiträge zum thermischen Verhalten wasserfreier Phosphate. IX. Darstellung und Kristallstruktur von $Cr_6(P_2O_7)_4$. Ein gemischtvalentes Pyrophosphat mit zwei- und dreiwertigem Chrom. Zeitschrift für Anorganische und Allgemeine Chemie, 616, 46–52.

——— (1993) Beiträge zum thermischen Verhalten wasserfreier Phosphate. VIII. Darstellung und Kristallstruktur von $Cr_7(PO_4)_6$. Das erste gemischtvalente Phosphat mit Cr(II) und Cr(III). Zeitschrift für Kristallographie, 205, 69–83.

Giester, G. and Rieck, B. (1994) Effenbergerite, $BaCu[Si_4O_{10}]$, a new

mineral from the Kalahari Manganese Field, South Africa: description and crystal structure. Mineralogical Magazine, 58, 663–670.

——— (1996) Wesselsite, $SrCu[Si_4O_{10}]$, a further new gillespite group mineral from the Kalahari Manganese Field, South Africa. Mineralogical Magazine, 60, 795–798.

Grant, D.F. and Gabe, E.J. (1978) The analysis of single-crystal Bragg reflections from profile measurements. Journal of Applied Crystallography, 11, 114–120.

Hazen, R.M. (1977) Mechanisms of transformation and twinning in gillespite. American Mineralogist, 62, 528–533.

Hazen, R.M. and Burnham, C.W. (1974) The crystal structures of gillespite I and II: a structure determination at high pressure. American Mineralogist, 59, 1166–1176.

Hazen, R.M. and Finger, L.W. (1983) High-pressure and high-temperature crystallographic study of the gillespite I-II phase transition. American Mineralogist, 68, 595–603.

Hitchman, M.A. (1985) Chemical information from the polarized crystal spectra of transition metal complexes. In G.A. Melson and B.N. Figgis, Eds., Transition Metal Chemistry, Vol. 9, p. 1–223. Marcel Dekker, New York.

Holzheid, A. and O'Neill, H.St.C. (1995) The Cr-Cr_2O_3 oxygen buffer and the free energy of formation of Cr_2O_3 from high-temperature electrochemical measurements. Geochimica Cosmochimica Acta, 58, 1975–1981.

Huggins, F.E., Mao, H.K., and Virgo, D. (1975) Mössbauer studies at high-pressures using the diamond-anvil cell. Carnegie Institute Year Book, 74, 405–410.

——— (1976) Gillespite at high-pressure: results of a detailed Mössbauer study. Carnegie Institute Year Book, 75, 756–758.

Ito, H., Ito, Y., Kanamura, F., Koto, K., Matsubayashi, N., Watanabe, I., and Ikeda, S. (1987) The crystal structure of chromium sulphate pentahydrate and the relation between the Jahn-Teller effect and cell dimensions. Zeitschrift für Kristallographie, 181, 99–107.

Janczak, J. and Kubiak, R. (1992) Refinement of the the structure of Barium Copper Silicate $BaCu[Si_4O_{10}]$ at 300K. Acta Crystallographica, C48, 1299–1301.

King, H.E. and Finger, L.W. (1979) Diffracted beam crystal centering and its application to high-pressure crystallography. Journal of Applied Crystallography, 12, 374–378.

Li, J.P., O'Neill, H.St.C., and Seifert, F. (1995) Subsolidus phase relations in the system $MgO-SiO_2-Cr-O$ in equilibrium with metallic Cr, and their significance for the petrochemistry of chromium. Journal of Petrology, 36, 107–132.

Lin, H.C., Liao, F.L., and Wang, S.L. (1992) Structure of $BaCuSi_4O_{10}$. Acta Crystallographica, C48, 1297–1299.

Miletich, R. and Allan, D.R. (1996) The gillespite-type Cr^{2+} silicates $BaCrSi_4O_{10}$ and $SrCrSi_4O_{10}$. (abs.) Zeitschrift für Kristallographie, Supplementum, 11, 88.

Maslen, E.N., Fox, A.G., and O'Keeffe, M.A. (1992) X-ray scattering. In A.J.C. Wilson, Ed., International Tables for Crystallography—Volume C, p. 476–509. Kluwer Academic Publishers, Dordrecht.

Nell, J. and de Villiers, J.P.R. (1993) T-pO_2 topologic analysis of phase relations in the system $CaO-CrO-Cr_2O_3-SiO_2$. Journal of American Ceramic Society, 76, 2193–2200.

Pabst, A. (1959) Structures of some tetragonal sheet silicates. Acta Crystallographica, 12, 733–739.

Ralph, R.L. and Finger, L.W. (1982) A computer program for refinement of crystal orientation matrix and lattice constants from diffractometer data with lattice symmetry constraints. Journal of Applied Crystallography, 15, 537–539.

Robinson, K., Gibbs, G.V., and Ribbe, P.H. (1971) Quadratic elongation: a qualitative measure of distortion in coordination polyhedra. Science, 172, 567–570.

Shannon, R.D. (1976) Revised effective ionic radii ans systematic studies of interatomic distances in halides and chalkogenides. Acta Crystallographica, A32, 751–767.

Strens, R.G.J. (1966) Pressure-induced spin-pairing in gillespite, $BaFe(II)Si_4O_{10}$. Chemical Communications, 21, 777–778.

Vaalsta, T.P. and Maslen, E.N. (1987) Electron Density in Chromium Sulfate Pentahydrate. Acta Crystallographica, B43, 448–454.

de Villiers, J.P.R. and Muan, A. (1992) Liquidus-solidus phase relationsship in the system $CaO-CrO-Cr_2O_3-SiO_2$. Journal of the American Ceramic Society, 75, 1333–1341.

Manuscript received December 8, 1996
Manuscript accepted February 28, 1997.